FEM-ANALYSIS OF CRACKS IN PIEZOELECTRIC STRUCTURES UNDER DYNAMIC ELECTROMECHANICAL LOADING

Marco Enderlein
Institute of Mechanics and Fluid Dynamics
Technische Universität Bergakademie Freiberg
Lampadiusstr. 4, 09596 Freiberg, Germany
Marco.Enderlein@imfd.tu-freiberg.de

Abstract

The behaviour of stationary cracks under combined electrical and mechanical dynamic loading conditions is important for many applications of piezoelectrics. To calculate electromechanical fracture quantities for structures with arbitrary shape and time dependent boundary conditions, numerical methods need to be used. In this paper a finite element algorithm is presented, which is based on an explicit time integration rule to solve the transient coupled electromechanical boundary value problem for a linear piezoelectric continuum. Furthermore numerical methods for the calculation of fracture quantities, for instance the dynamic electromechanical J-Integral, are described. Results for a plane crack problem under different loading conditions are presented and discussed.

Introduction

In order to improve the functional features and the mechanical properties of piezoelectric structures fracture mechanics concepts are gaining growing interest. The macroscopic failure of piezoelectric ceramics is mainly determined by growth of microscopic cracks. Here, mechanical and electrical field intensity factors and energy release rates play an important role as fracture quantities. However, the dynamic aspect in fracture mechanics of these structures is rarely investigated. The behaviour of stationary cracks under combined electrical and mechanical dynamic loading conditions is important for many applications of piezoelectrics, though. For instance in ultrasonic transducers the excitation frequencies are close to or above the lowest eigenfrequency of the structure, so that dynamic effects cannot be neglected. In other applications, such as sensors and actors smart ceramics often underlie electrical or mechanical impact loading. Therefore, methods have to be developed allowing the calculation of dynamic field intensity factors and energy release rates.

To calculate electromechanical fracture quantities for structures with arbitrary shape and time dependent boundary conditions, numerical methods such as the Finite Element method (FEM) need to be used. At present, commercial FEM codes are available for static piezoelectric analysis, only. Moreover, fracture mechanical tools as e.g. the electromechanical J-Integral are not implemented. Therefore, an explicit finite element program has been developed containing tools, allowing an efficient calculation of dynamic fracture quantities.

Finite element algorithm for piezoelectric problems

The constitutive equations for a piezoelectric continuum are given by:

$$\sigma_{ij} = c_{ijkl}\varepsilon_{kl} - e_{kij}E_k \,, \tag{1}$$

$$D_i = e_{ikl}\varepsilon_{kl} + \kappa_{ik}E_k\,, \tag{2}$$

where σ_{ij} is the stress tensor, D_i is the electric displacement vector and c_{ijkl}, e_{kij}, κ_{ik} are the elastic, piezoelectric and dielectric material tensors, Parton and Kudryavtsev [1], Tiersten [2], Qin [3], Zhang [4]. The strain tensor ε_{kl} and the electric field vector E_k are defined as:

$$\varepsilon_{kl} = \frac{1}{2}\left(u_{k,l} + u_{l,k}\right), \tag{3}$$

$$E_k = -\varphi_{,k}\,. \tag{4}$$

Applying Hamiltons principle the corresponding coupled electromechanical boundary value problem can be described in a weak form:

$$\int_{t_0}^{t}\int_{V}\left(D_i\delta E_i - \rho\ddot{u}_i\delta u_i - \sigma_{ij}\delta\varepsilon_{ij} + b_i\delta u_i - \omega^v\delta\varphi\right)dVdt + \int_{t_0}^{t}\int_{S}\left(t_i^s\delta u_i - \omega^s\delta\varphi\right)dSdt = 0. \tag{5}$$

Here b_i and ω^v denote prescribed body forces and body charges. With t_i^s and ω^s applied external stresses and charge densities acting on the boundary S are considered. Since the variations of the independent variables δu_i and $\delta\varphi$ are arbitrary inside the volume V and on the boundary S, the Fundamental Lemma of variational calculus yields the Euler-Lagrangian equations, i.e. the equilibrium conditions of elastodynamics

$$\sigma_{ij,j} + b_i - \rho\ddot{u}_i = 0 \tag{6}$$

and electrostatics

$$D_{i,i} - \omega^v = 0 \tag{7}$$

as well as the natural boundary conditions on the surface S

$$\sigma_{ij}n_j = t_i^s\,,\; D_i n_i = -\omega^s\,, \tag{8}$$

with n_i as the outer unit normal vector to S. In terms of a finite element approximation Eqn. (6)-(8) can be written as two equilibrium equations:

$$\underline{\mathbf{m}}\ddot{\mathbf{u}} + \underline{\mathbf{k}}_{uu}\mathbf{u} + \underline{\mathbf{k}}_{u\varphi}\boldsymbol{\varphi} = \mathbf{f}_b + \mathbf{f}_s + \mathbf{f}_p \tag{9}$$

$$\underline{\mathbf{k}}_{\varphi u}\mathbf{u} + \underline{\mathbf{k}}_{\varphi\varphi}\boldsymbol{\varphi} = \mathbf{q}_b + \mathbf{q}_s + \mathbf{q}_p\,, \tag{10}$$

where $\underline{\mathbf{m}}$ denotes the mass matrix and $\underline{\mathbf{k}}_{uu}$, $\underline{\mathbf{k}}_{u\varphi}$ and $\underline{\mathbf{k}}_{\varphi\varphi}$ are the mechanical, the dielectrical and the piezoelectrical stiffness matrices. The vectors $\mathbf{u}$ and $\boldsymbol{\varphi}$ are the unknown nodal displacements and electrical potential, respectively. The right hand side of Eqn. (9) and (10) comprises the nodal vectors of prescribed loads and charges.

An explicit time integration scheme is used, to solve the system of differential equations. With the central difference integration operator:

$$\begin{aligned}\dot{\mathbf{u}}^{n+\frac{1}{2}} &= \dot{\mathbf{u}}^{n-\frac{1}{2}} + \frac{\Delta t^{n+1} + \Delta t^n}{2}\ddot{\mathbf{u}}^n\\ \mathbf{u}^{n+1} &= \mathbf{u}^n + \Delta t^{n+1}\dot{\mathbf{u}}^{n+\frac{1}{2}}\end{aligned}\,, \tag{11}$$

Eq. (9) can be rewritten:

$$\frac{2}{\Delta t^{n+1}}\underline{\mathbf{m}}\mathbf{u}^{n+1}=\left(\mathbf{f}_b+\mathbf{f}_s+\mathbf{f}_p-\underline{\mathbf{k}}_{uu}\mathbf{u}^n-\underline{\mathbf{k}}_{u\varphi}\boldsymbol{\varphi}^n\right)\left(\Delta t^{n+1}+\Delta t\right)+2\underline{\mathbf{m}}\left(\frac{\mathbf{u}^n}{\Delta t^{n+1}}+\frac{\mathbf{u}^{n-1}}{\Delta t^n}\right). \tag{12}$$

Here $\dot{\mathbf{u}}$ and $\ddot{\mathbf{u}}$ are the velocity and the acceleration, respectively. The superscript n refers to the increment number and $n\pm\frac{1}{2}$ to the midincrement values. The electrical potential $\boldsymbol{\varphi}^{n+1}$ is calculated from Eq. (10):

$$\underline{\mathbf{k}}_{\varphi\varphi}\boldsymbol{\varphi}^{n+1}=\mathbf{q}_b^{n+1}+\mathbf{q}_s^{n+1}+\mathbf{q}_p^{n+1}-\underline{\mathbf{k}}_{u\varphi}\mathbf{u}^{n+1}. \tag{13}$$

For the element mass matrices a lumped formulation, Wriggers [5], is used, whereby the inversion of $\underline{\mathbf{m}}$ at the beginning of every increment becomes trivial. Thus the explicit algorithm shows a very high computational efficiency. Problems arise from the limited stability of the algorithm and from numerical effects, which occur in the simulation of high-speed dynamic events. Therefore, appropriate procedures for time step control associated with artificial viscosity need to be used, ABAQUS [6], Wilkins [7].

Fracture mechanics of piezoelectrics

Mechanical and electrical intensity factors, energy release rate

The asymptotic $1/\sqrt{r}$ behaviour of stresses σ_{ij} and electric displacements D_i in the vicinity of a crack tip can be described in terms of the stress intensity factors K_I, K_{II}, K_{III} and the electric intensity factor K_{IV}, Pak [8], Sosa and Pak [9]:

$$\begin{aligned}(r,\theta)&=\frac{1}{\sqrt{2\pi r}}\left[K_I f_{ij}^{I}(\theta)+K_{II} f_{ij}^{II}(\theta)+K_{III} f_{ij}^{III}(\theta)+K_{IV} f_{ij}^{IV}(\theta)\right]\\(r,\theta)&=\frac{1}{\sqrt{2\pi r}}\left[K_I g_i^{I}(\theta)+K_{II} g_i^{II}(\theta)+K_{III} g_i^{III}(\theta)+K_{IV} g_i^{IV}(\theta)\right].\end{aligned} \tag{14}$$

Here r and θ denote the distance from and the angle around the crack tip, see Fig. 1, $f_{ij}(\theta)$ and $g_i(\theta)$ are angular functions characterising the asymptotic near field distribution. Another value describing the loading of the crack is the energy release rate, which is defined as the change of the total energy Π related to an incremental growth of the crack area ΔA:

$$G=-\lim_{\Delta A\to 0}\left(\frac{\Delta\Pi}{\Delta A}\right)=-\frac{d\Pi}{dA}. \tag{15}$$

The energy release rate and the intensity factors are related by a generalised Irwin relationship:

$$G=\frac{1}{2}K_M K_N Y_{MN}\qquad M,N=\{I,II,III,IV\} \tag{16}$$

where $K_M=\left(K_{II},K_I,K_{III},K_{IV}\right)^T$ and Y_{MN} is the Irwin matrix, depending on the material tensors c_{ijkl}, e_{kij}, κ_{ik} and the orientation of the crack with respect to the material axes, Suo *et al.* [10].

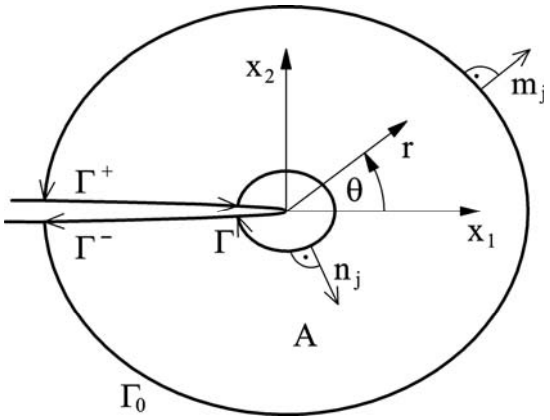

FIGURE 1. Crack tip coordinates and integration contours.

Dynamic piezoelectric J-integral

The J-integral is a very powerful method for the numerical calculation of the energy release rate. For an elastic piezoelectric material the J-Integral vector can be written as an integral along the closed contour Γ around the crack tip, see Fig. 1, Cherepanov [11]:

$$J_k = \lim_{\Gamma \to 0} \int_{\Gamma} \left[\left(H + T \right) \delta_{kj} - \sigma_{ij} u_{i,k} + D_j E_k \right] n_j d\Gamma \,. \tag{17}$$

Here H denotes the electrical enthalpy density, which is given by:

$$H = \frac{1}{2} \left(\sigma_{ij} \varepsilon_{ij} - D_i E_i \right). \tag{18}$$

T means the kinetic energy density, n_j the unit vector normal on Γ pointing outward of the enclosed domain and δ_{kj} is the unit tensor. Regarding only the x_1-component of J_k, which has the physical meaning of G for two-dimensional problems and restricting to the case of a stationary crack, then Eq. (17) reduces to:

$$J_1 = G = \lim_{\Gamma \to 0} \int_{\Gamma} \left(H \delta_{1j} - \sigma_{ij} u_{i,1} + D_j E_1 \right) n_j d\Gamma \,. \tag{19}$$

To evaluate J_1 in a finite element analysis, Eq. (19) conveniently is transformed into an equivalent domain integral using the virtual crack extension technique, Abendroth *et al.*[12], Hellen [13]. Following this method:

$$J_1 = \int_A \left[\left(\sigma_{ij} u_{i,1} - D_j E_1 - H \delta_{1j} \right) q_{,j} + \rho \ddot{u}_i u_{i,1} q \right] dA, \tag{20}$$

where q is an arbitrary smooth weighting function, which has the value one on the inner contour Γ and zero on the outer contour Γ_0, see Fig. 1. Eq. (20) holds for traction and charge free crack surfaces and omitting body forces and charges as well as property gradients. It can be easily implemented in a finite element program or in a postprocessor calculating the integral numerically. Due to the path independence of the J-integral the produced results are highly accurate and rarely sensitive to the quality of the numerical solution in the vicinity of the crack tip singularity. A drawback is that the separation of the stress intensity factors and electric intensity factors from J is not straightforward.

Near tip solution and extraction of intensity factors

The intensity factors K_N can be calculated from the near tip fields of the displacements u_i and the electric potential φ. On the crack faces ($\theta = \pm\pi$) it is:

$$\begin{pmatrix} u_i \\ \phi \end{pmatrix} = \pm\sqrt{\frac{2r}{\pi}} Y_{MN} K_N \quad (r \to 0). \tag{21}$$

Considering just Mode-I/Mode-IV loading conditions the field intensity factors are calculated from displacements and electrical potentials on the positive crack, see e.g. Kuna [14]:

$$\begin{aligned} K_I &= \sqrt{\frac{\pi}{2r}} \left(\frac{c_T e^2}{c_T \kappa + e^2} u_2^+ + \frac{c_T e \kappa}{c_T \kappa + e^2} \varphi^+ \right) \\ K_{IV} &= \sqrt{\frac{\pi}{2r}} \left(\frac{c_T e \kappa}{c_T \kappa + e^2} \varphi^+ - \frac{e^2 \kappa}{c_T \kappa + e^2} u_2^+ \right), \end{aligned} \tag{22}$$

where c_T, e, and κ are constants of the Irwin matrix. In terms of a finite element analysis Eq. (22) can be evaluated using u_2^+ and φ^+ at the nodes on the crack face close to the tip. This makes it a very easy method for the calculation of the intensity factors. However, it has to be stated that the results strongly depend on the quality of the finite element solution, which in most cases is not very accurate in the vicinity of the crack tip.

Combination of the near tip solution and the J-integral

In order to increase the accuracy of the aforementioned method, it is combined with the J-integral. Taking the ratio $R = K_{IV}/K_I$ from the near tip solution, Eq. (22), and the energy release rate G from the J-integral method, inserting both in Eq. (16) yields:

$$\begin{aligned} \tilde{K}_I &= \sqrt{\frac{2G}{\frac{1}{c_T} - \frac{R^2}{\kappa} + \frac{2R}{e}}} \\ \tilde{K}_{IV} &= R \cdot \tilde{K}_I \end{aligned} . \tag{23}$$

This is a very simple method to separate the intensity factors from the J-integral, leading to acceptable results in many cases. However, calculations have also shown that the method is not reliable in general and sometimes produces unstable results.

Permeability of the crack

For electromechanical crack analyses the limited permeability of the crack, i.e. the influence of a dielectric medium inside the crack, needs to be considered. The models of the impermeable and the fully permeable crack can be regarded only as simple approximations representing upper and lower bounds for the electrical energy penetrating the crack. The finite element realisation of the limited permeable crack for static problems is based on an iterative procedure, Wippler *et al.* [15], Hao and Shen [16], McMeeking [17]. However, this method proved to be not favourable for crack dynamics. For the problems analysed here a special technique is used, meshing the inside of the crack with dielectric capacitor elements of variable length depending on the local crack opening.

Numerical examples

The subject under consideration is a central through-thickness crack of the length $2a$ in a rectangular sheet, made of barium titanate, see Fig. 2. The material is poled in positive x_2-direction. At the opposite ends of the bar mechanical and electrical loads $\sigma_0(t)$ and $D_0(t)$ are applied following a step function with the time constant $\tau = 1 \cdot 10^{-6}\,\mathrm{s}$. For the finite element discretisation a two-dimensional model of quadrilateral elements with linear shape functions is used. Because of symmetry only a quarter of the plate had to be modelled. On the ligament symmetry boundary conditions $u_2 = 0$ and $\varphi = 0$ are applied and along the vertical symmetry line holds $u_1 = 0$.

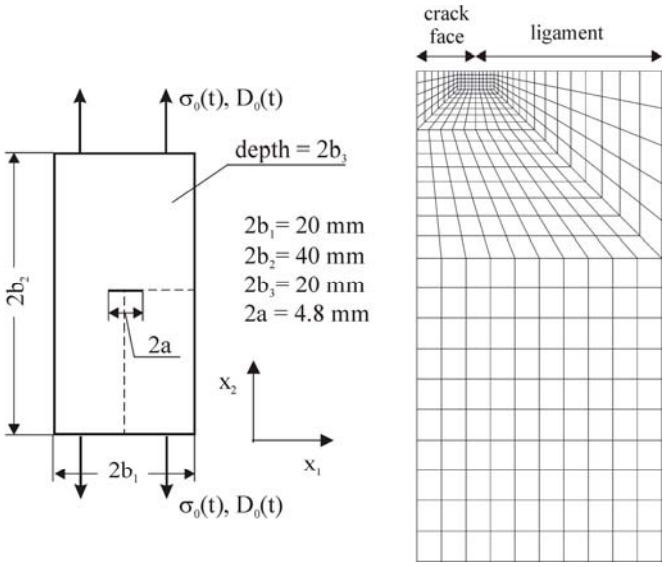

FIGURE 2. Rectangular bar containing a central through-thickness crack.

In Fig. 3 the calculated J-integral is plotted vs. time. The first curve (dotted line) stands for the described model without any further modifications. The crack is modelled as impermeable. As can be seen the J-integral first decreases for $t \le \tau$ remaining at approx. the same level till $t \approx 4.0 \cdot 10^{-6}$ s. During this period the electrical field, which emerged immediately into the body dominates the behaviour of the crack. Regarding the displacements at the crack face in this state a positive u_2 is found, meaning a non-physical penetration of the crack faces. After that period the stress wave induced by σ_0 and D_0 at the bottom of the model has reached the crack, what results in a steep increase of the curve with a maximum at $t \approx 9.0 \cdot 10^{-6}$ s. After that the curve decreases again. To avoid the penetration of the crack faces at the beginning of the simulation, contact boundary conditions have to be introduced. This can be realised very simply for the symmetric model, allowing only negative displacements u_2 at the crack face. Furthermore, the condition $\varphi = 0$ has to be set for all nodes along the crack face as long as $u_2 = 0$. The results of the simulation under these conditions are represented by the dashed line in Fig. 3. Here, the J-integral remains at zero for $t < \tau$, since the closed crack is invisible (fully permeable) for the electric field. When the crack opens a steep drop of the curve is observed, caused by the sudden change to the boundary conditions of an impermeable crack. As time develops the curve shows a similar behaviour as the dotted line. The third curve (solid line) in Fig. 3 represents the case if the crack is modelled as limited permeable in combination with the contact conditions at the crack face. Compared to the dashed curve the steep drop at $t \approx 4.0 \cdot 10^{-6}$ s is not found here because of the variable permeability in the interior of the crack. However, if the limited

permeable crack model is used the crack faces can not be treated as charge free and consequently Eq. (20) is not valid anymore. To get correct results surface integrals (line integrals for 2D-problems) along the crack faces need to be accounted for in the calculation of *J*. These have not been implemented in the program yet.

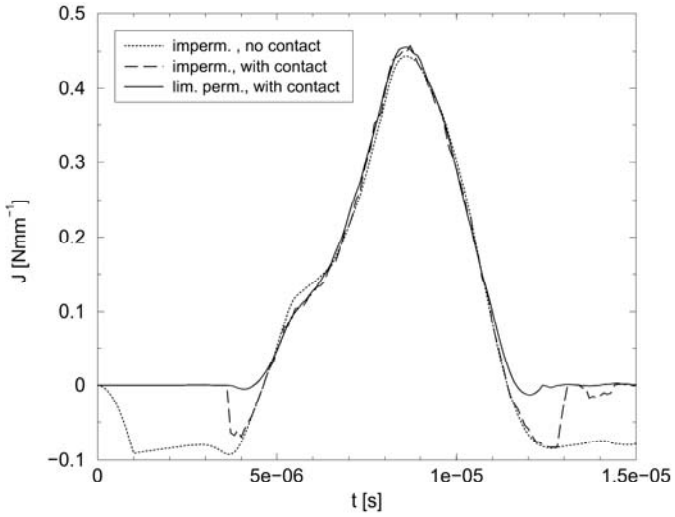

FIGURE 3. J-integral vs. time for different crack configurations.

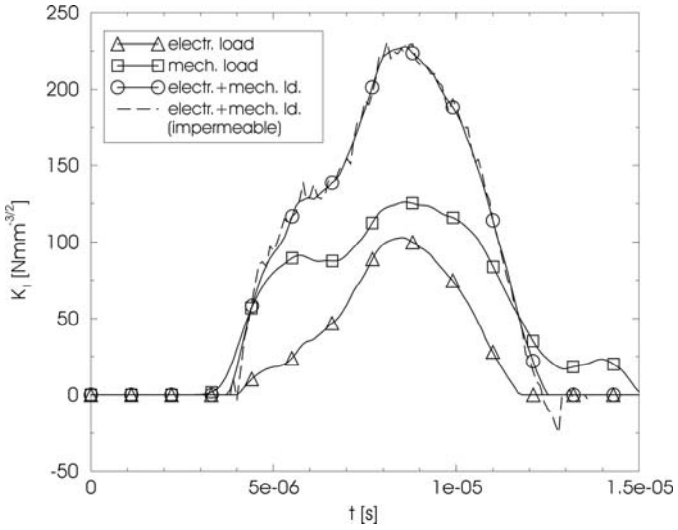

FIGURE 4. K_I vs. time for different load cases.

In Fig. 4 the stress intensity factor K_I is plotted vs. time for three different load cases: (i) $D_0(t)$, (ii) $\sigma_0(t)$, (iii) $D_0(t),\sigma_0(t)$. The crack is modelled as limited permeable with crack face contact for these calculations. K_I is computed from the near tip field solution, Eq. (22). As can be seen all curves are zero before $t = \tau$ showing a maximum at $t \approx 9.0 \cdot 10^{-6}$ s. The highest value of K_I is reached under electrical and mechanical loading conditions. It is worth to be noted that contrary to the according static problem for a pure electrical load a nonzero K_I exists. Regarding the electrical mode, see Fig. 5, a nonzero K_{IV} occurs for all load cases. This effect is caused by the variable permeability inside the crack, depending on the actual crack opening and is found for static calculations, too. In Fig. 4 and 5 the results for the impermeable crack are given as dashed lines. As expected an influence is found only for K_{IV}.

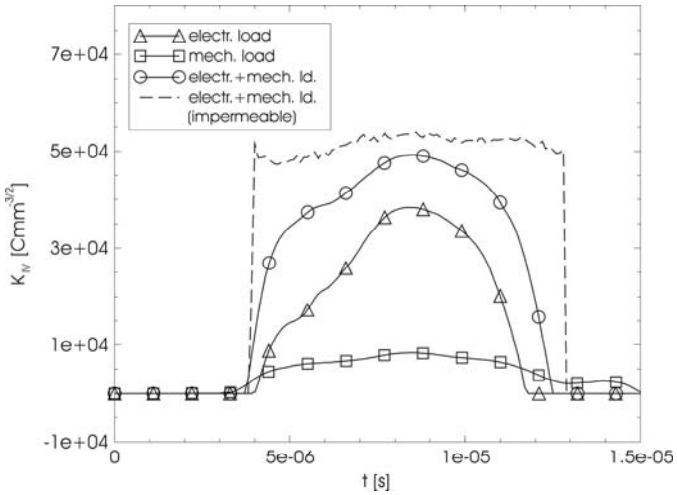

FIGURE 5. K_{IV} vs. time for different load cases.

Conclusions

An explicit finite element program for the investigation of dynamic piezoelectric problems has been developed. Basic fracture mechanical tools are implemented into the code. First results have been presented for impermeable and limited permeable crack configurations, exposed to dynamic electromechanical step loading.

References

1. Parton, V. Z., Kudryavtsev, B. A., *Electromagnetoelasticity, Piezoelectrics and Electrically Conductive Solids*, Gordon and Breach Science Publishers, New York, 1988
2. Tiersten, H. F., *Linear Piezoelectric Plate Vibrations*, Plenum Press, New York, 1964
3. Zhang, T.-Y., *Advances in Applied Mechanics*, vol. **38**, 147-289, 2002
4. Qin, Q.-H., *Fracture Mechanics of Piezoelectric Materials*, WIT Press, Southampton, Boston, 2001
5. Wriggers, P., *Nichtlineare Finite-Elemente-Methoden*, Springer, Berlin, Germany, 2001
6. ABAQUS, *Theory Manual, Version 5.8*, Hibbitt, Karlson & Sorensen, Inc., 1998
7. Wilkins, M. L., *J. Comp. Phys.*, vol. **36**, 281, 1980
8. Pak, Y. E., *Int. J. Frac.*, vol. **54**, 79-100, 1992
9. Sosa, H. A., Pak, Y. E., *Int. J. Solids Struct.*, vol. **26**, 1-15, 1990
10. Suo, Z., Kuo, C.-M., Barnett, D. M., Willis, J. R., *J. Mech . Phys. Solids*, vol. **40**, 739-765, 1992
11. Cherepanov, G. P., *Nauka*, Moscow, 1974, English transl.: McGraw-Hill, 1979
12. Abendroth, M., Groh, U. Kuna, M. Ricoeur, *Int. J. Frac.*, vol. **114**, 359-378, 2002
13. Hellen, T. K., *Comp. Meth. Appl. Mech. Engng.*, vol. **12**, 353-364, 1975
14. Kuna, M., *Comp. Materials Science*, vol. **13**, 67-80, 1998
15. Wippler, K., Ricoeur, A., Kuna, M., to appear in: *Engng. Frac. Mech.*, 2004
16. Hao. T., Shen, Z., *Engng. Frac. Mech.*, vol. **47**, 793-802, 1994
17. McMeeking, R., *Engng. Frac. Mech.*, vol. **64**, 217-244, 1999